

Complex magnetism of the two-dimensional antiferromagnetic Ge_2F : from a Néel spin-texture to a potential antiferromagnetic skyrmion

Fatima Zahra Ramadan¹, Flaviano José dos Santos², Lalla Btissam Drissi^{1,2,3}, Samir Lounis^{2,4}

¹*LPHE-Modeling and Simulation, Faculty of Sciences, University Mohammed V, Rabat, Morocco*

²*Peter Grünberg Institut and Institute of Advanced Simulation, Forschungszentrum Jülich & JARA, D-52428, Jülich, Germany*

³*CPM, Centre of Physics and Mathematics, Faculty of Science, Mohammed V University in Rabat, Rabat, Morocco*

⁴*Faculty of Physics, University of Duisburg-Essen, 47053 Duisburg, Germany*

Abstract

Based on density functional theory combined with low-energy models, we explore the magnetic properties of a hybrid atomic-thick two-dimensional (2D) material made of Germanene doped with fluorine atoms in a half-fluorinated configuration (Ge_2F). The Fluorine atoms are highly electronegative, which induce magnetism and break inversion symmetry, triggering thereby a finite and strong Dzyaloshinskii-Moriya interaction (DMI). The magnetic exchange interactions is of antiferromagnetic nature among the first, second and third neighbors, which leads to magnetic frustration. The Néel state is found to be the most stable state, with magnetic moments lying in the surface plane. This results from the out-of-plane component of the DMI vector, which seems to induce an effective in-plane magnetic anisotropy. Upon application of a magnetic field, spin-spirals and antiferromagnetic skyrmions can be stabilized. We conjecture that this can be realized via magnetic exchange fields induced by a magnetic substrate. To complete our characterization, we computed the spin-wave excitations and the resulting spectra, which could be probed via electron energy loss spectroscopy, magneto-Raman spectroscopy or scanning tunneling spectroscopy.

Keywords Germanene; first principles calculations; Spin-wave; Skyrmions; Dzyaloshinskii-Moriya interaction (DMI); Wannier functions.

1 Introduction

The realization of complex spin-textures hinges on the presence of competing magnetic interactions, which are heavily explored in various materials. While hosting fundamentally exciting phenomena, such magnetic states have great potential in spintronics with possible impact on information technology. For example, going beyond the conventional ferromagnetic (FM) materials for practical applications, such as the antiferromagnetic (AFM) ones [2, 3, 4, 1] can have various interesting advantages. AFMs are expected to be robust against perturbation due to magnetic fields, they produce no stray fields, display ultrafast dynamics, and are capable of generating large magnetotransport effects [1].

The emergence of complex magnetic states is favored by the presence of competing magnetic interactions, which can lead to frustration. Spin-orbit driven interactions, such as the Dzyaloshinskii-Moriya Interaction (DMI), also favor non-collinearity with the additional injection of a potential chiral magnetic behavior. Indeed, broken inversion symmetry and spin-orbit coupling triggers a finite DMI, which stabilizes a unique sense of rotation of the magnetic moments. Various chiral spin-swirling states can then be produced, such as chiral spin spirals, chiral domain walls or magnetic skyrmions. The latter are topological protected vortex lines in which the spins point in all the directions wrapping a sphere [5, 6, 7], which are promising for potential high-density and low-power spintronics technology [8, 10, 9]. In this field, there is currently a great interest in going beyond FM skyrmions by discovering AFM skyrmions[11, 12, 13, 14, 15, 16, 17, 18], which would combine the advantages of skyrmions[19, 20, 21, 25, 22, 23, 24] and AFM properties.

The goal of this manuscript is to prospect the presence of chiral complex spin textures in two dimensional (2D) magnetic materials. They not only offer unique physical and chemical properties, but also an unprecedented flexibility in system design. When grown in a multilayer fashion, their flexibility stems from van-der-Waals bonding between neighboring atomic-thick layers of potentially very different properties, which permits virtually unlimited combinations and stackings of individual layers. The resulting properties, usually conveyed via proximity effects, can be very distinct from the original building block materials. Most of 2D materials do not exhibit DMIs because of their centrosymmetric crystal structure.

To break such a symmetry, some approaches consist on creating 2D structures within which different atoms are mixed in an alternating manner to generate one-atom thick hybrids [36, 26, 27]. Other strategies such as applying a bias voltage or strain are also used [28, 29, 30]. Chemical functionalization, impurities, boundaries and defects are other efficient ways employed in 2D sheets to tune their physical properties and induce magnetic order [32, 31, 34, 29, 35, 33]. In particular, chemisorption using radicals such as oxygen, hydrogen or fluorine atoms on the surface of 2D honeycomb structures leads to long-range magnetism [36, 37, 38, 39, 40]. Another example consists of Sn monolayer on SiC(0001) surface, where a strong spin-orbit coupling was found on the basis of a generalized Hubbard model. This mainly contributes in the formation of a nanoskyrmion state at realistic magnetic fields and temperatures [41].

Half-functionalization is also a powerful and widely-used tool to tailor spin and magnetic behavior in 2D materials [42, 43]. A particularly interesting adatom is fluorine since it is the most electronegative element of the periodic table. Half fluorination is an exothermic adsorption that generates stable 2D hexagonal structures [44]. In half-fluorinated graphene, C_2F , where F-atoms form strong covalent bonds

with carbon, a threshold of the antiferromagnetic-ferromagnetic instability with strong Dzyaloshinskii-Moriya interaction was predicted [46] with the potential presence of ferromagnetic skyrmions. The latter work challenged the ab-initio results obtained by Rudenko et al. [45], which revealed finite AFM interactions on the triangular lattice of magnetic moments, leading to the instability of the collinear magnetic ordering due to frustration and the stabilization of a 120° Néel state. Mazurenko et al. [46] proposed that the direct exchange interaction between spin orbitals, not accounted in Ref. [45], leads to a ferromagnetic interaction, which is capable of compensating the antiferromagnetic indirect exchange interactions in C_2F .

Remarkably, half-fluorination can trigger opposite magnetic behavior in hybrid 2D monolayers. While half-fluorinated BN sheet is an antiferromagnetic direct semiconductor, half-fluoro-GaN monolayer shows ferromagnetic character [47]. In silicene-graphene (SiC), interesting magnetic properties can emerge depending on which host atom (C or Si) fluorine is attached [48].

In this paper, we study the presence of chiral spin-textures in half fluorinated germanene using density functional theory (DFT) combined with low-energy models with spin-orbit coupling in the spirit of the methodology followed by Mazurenko et al. [46]. We found that the Ge_2F is antiferromagnetic with strong DMI between the first nearest magnetic germanium neighbors. The spin dynamics simulations demonstrate the stability of the antiferromagnetic Néel state, resulting from magnetic frustration. In the latter configuration, the magnetic moments lie in the surface plane, which is induced by the out-of-plane component of the DMI vector. Extremely large magnetic fields can stabilize an antiferromagnetic skyrmion. We conjecture that this can be enabled by a proximity-effect induced by an underlying magnetic substrate. Noting that magnons in 2D structures have been probed with magneto-Raman spectroscopy [49] and scanning tunneling microscopy [50], we finally explore the spin-wave excitations characterizing the obtained complex spin-textures.

2 Computational details

The electronic and magnetic properties have been obtained using the Quantum espresso code [51], which is based on density functional theory (DFT). Exchange and correlation effects were taken into account using the local spin density approximation (LDA). Spin-orbit (SO) coupling was included on the basis of fully relativistic pseudopotentials. In these calculations, we set the energy cutoff to $60Ry$ for the plane-wave basis. For the Brillouin-zone integration a $30 \times 30 \times 1$ Monkhorst Pack mesh was used. To avoid the artificial interactions between layers, the thickness of the vacuum space was fixed at 20\AA . To extract the magnetic exchange interactions required for the exploration of the magnetic properties, we built a low-energy model using an effective Hamiltonian following the work of Mazurenko et al. [46]:

$$\hat{H} = \sum_{ij,\sigma\sigma'} t_{ij}^{\sigma\sigma'} \hat{a}_{i\sigma}^\dagger \hat{a}_{j\sigma'} + \frac{1}{2} \sum_{i,\sigma\sigma'} U_{00} \hat{a}_{i\sigma}^\dagger \hat{a}_{i\sigma'}^\dagger \hat{a}_{i\sigma'} \hat{a}_{i\sigma} + \frac{1}{2} \sum_{i,\sigma\sigma'} U_{ij} \hat{a}_{i\sigma}^\dagger \hat{a}_{i\sigma'}^\dagger \hat{a}_{i\sigma'} \hat{a}_{i\sigma} + \frac{1}{2} \sum_{i,\sigma\sigma'} J_{ij}^F \hat{a}_{i\sigma}^\dagger \hat{a}_{i\sigma'}^\dagger \hat{a}_{i\sigma'} \hat{a}_{i\sigma} \quad (1)$$

where $i(j)$ and $\sigma(\sigma')$ are site and spin indices, $\hat{a}_{i\sigma}^\dagger$ ($\hat{a}_{j\sigma'}$) are the creation (annihilation) operators, and U_{00} , U_{ij} and J_{ij}^F represent local Coulomb, non-local Coulomb and non-local ($i \neq j$) exchange interactions, respectively, and are obtained using the constrained random phase approximation (cRPA) [52] as implemented in the ABINIT code [53]. t_{ij} is a hopping matrix-element taking into account the

spin-orbit coupling, which is determined using the Wannier parameterization for the three nearest neighbours. To parameterize the (DFT+SO) spectra and construct the corresponding low-energy model, we use maximally localized Wannier functions, implemented in the wannier90 package [54].

Moreover, we used the Spirit atomistic spin dynamics simulation code [55] to solve the Landau-Lifshitz-Gilbert (LLG) equation:

$$\frac{d\mathbf{M}_i}{dt} = -\gamma\mathbf{M}_i \times \mathbf{B}_i^{\text{eff}} + \frac{\alpha}{M_i}\mathbf{M}_i \times \frac{\partial\mathbf{M}_i}{\partial t} \quad (2)$$

where γ is the electronic gyromagnetic ratio, α the damping factor, and \mathbf{M}_i is the magnetic moment at a given site i . This permits the investigation of the magnetic properties of Ge₂F described by an extended Heisenberg Hamiltonian given in eq. 5, with $\mathbf{B}_i^{\text{eff}} = -\frac{\partial H}{\partial \mathbf{M}_i}$. We assume a supercell of a size of $100 \times 100 \times 1$ atoms.

Once the ground state or a metastable state is found, we compute the adiabatic spin-wave modes and the corresponding inelastic scattering spectrum, based on time-dependent perturbation theory. The associated theoretical framework was presented in Refs.[56, 57] and used for various problems [58, 59]. The spin-wave eigenvalues $\omega_{\mathbf{k}}$ and eigenvectors K are then obtained after diagonalization of the system's dynamical matrix in the reciprocal space. We arrive to the total dynamical structure factor (summing up all the scattering channels), which is given by

$$\Gamma(\mathbf{q}, \omega) \propto \sum_{\alpha} \sum_{\mu\nu} e^{i\mathbf{q}\cdot\mathbf{R}_{\mu\nu}} \mathcal{N}_{\mu\nu}^{\alpha\alpha}(\mathbf{q}, \omega) \quad , \quad (3)$$

where $\alpha, \beta = x, y, z$ and μ, ν are site indices for spins in the unit cell that encompasses the noncollinear ground state magnetic structure. The spin-spin correlation tensor can be expressed using the information about the spin-wave modes as

$$\mathcal{N}_{\mu\nu}^{\alpha\beta}(q, \omega) = \sum_{k,r} \delta(\omega - \omega_r(k)) \langle 0 | S_{\mu}^{\alpha(-q)} | k, r \rangle \langle k, r | S_{\nu}^{\beta}(q) | 0 \rangle, \quad (4)$$

where $\omega_r(\mathbf{k})$ is the energy of the spin-wave mode r with wavevector \mathbf{k} , and matrix elements of the spin operators between the ground state and the excited spin-wave states [57].

Within this framework we have access to several distinct scattering channels. In this work we present results for the total inelastic scattering spectrum due to spin waves (the sum over all scattering channels), as one would measure in an experiment with an unpolarized scattering experiment such as electron energy loss spectroscopy (EELS). The various scattering channels will also be analyzed, which could be detected via the recent theoretical proposal, spin-resolved EELS (SREELS), shown in Ref. [57]. Within the latter, a spin-polarized beam of electrons is used to probe the magnetic material. The scattered electrons are then spin-filtered with the spin analyzer collinear with the incident beam polarization. This gives rise to four scattering channels, one for each possible combinations of [incoming spin]-[outgoing spin]. Two of these channels correspond to non-spin-flip processes, namely the up-up and the down-down channels. The other two, up-down and down-up, account for spin-flip events, where angular momentum is exchanged with the sample.

3 Results and discussion

In this paper, we study the magnetic properties of 2D half-fluorinated germanene where F-atoms bind Ge-atoms occupying the A-sites of each hexagonal lattice while B-sites remain undecorated

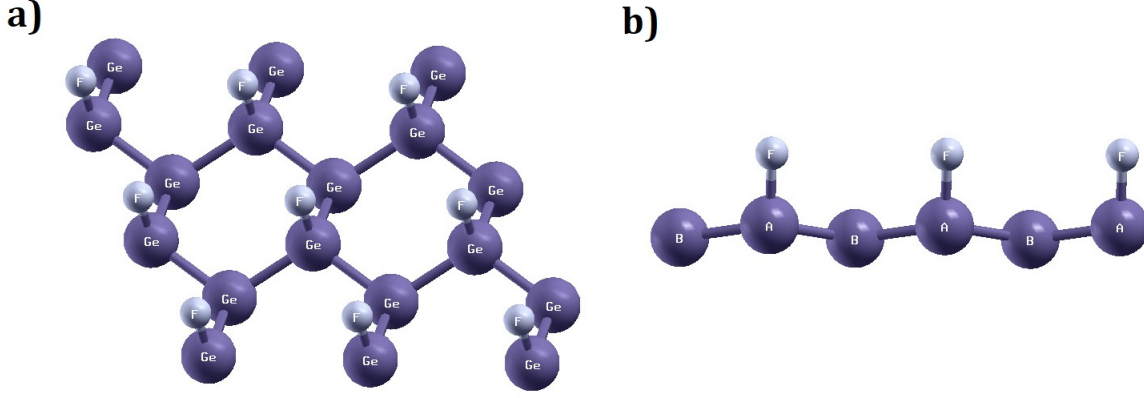


Figure 1: Optimized configuration (a) top (b) side of half-fluorinated germanene Ge_2F . Fluor (small spheres) atoms binds to Germanium atoms (site A), while Germanium atoms at site B are undecorated (as shown in the side view configuration).

as shown in Fig. 1. The bond lengths are $d_{\text{Ge-Ge}} = 2.52 \text{ \AA}$ and $d_{\text{Ge-F}} = 1.80 \text{ \AA}$. The structure is slightly puckered, with a buckling parameter of 0.74 \AA . The interatomic angles ranging between 111.70° and 111.80° indicate an sp^3 hybridization between Ge atoms. According to Ref. [60], the Ge_2F is an antiferromagnetic semiconductor, which a small gap energy. To check and examine the stability of free-standing monolayer materials, various computational methods can be used such as molecular dynamics [62, 61], the computation of formation energy and binding energy [60], as well as translational symmetry based on the relaxation of a finite nanocluster [63, 64]. In this work, the stability of half fluorinated germanene, confirmed in [60] calculating the formation energy, is rechecked through the analysis of the phonon dispersion, the figure 2 displays the phonons dispersion. Analysis of the phonon spectrum shows the absence of imaginary frequency along the high-symmetry directions of the Brillouin zone for all phonon branches. It is a signature of stability of our material. Fig. 3 (a) illustrates the LDA band-structure, including SO coupling. The metallic character of Ge_2F is in good agreement with recent work [66]. As expected, a small gap energy of 0.19eV is reported for Ge_2F using the generalized gradient approximation (GGA) [60]. It is worth noting that the standard DFT approximations, namely the LDA and the GGA, are known to successfully describe the ground-state properties and to underestimate the results of excited states. Thus to include quasiparticle corrections, which reproduce a band gap in accordance with the experimental measurements, one should use the GW approximation that goes beyond the scope of this work [68, 67]. Fig. 3 (a) also shows the bands around the Fermi level slightly overlap with other bands at the Γ -point similarly to what was found for the half fluorinated graphene (C_2F) [46] but with a larger spin-orbit splitting induced by the heavier Ge atoms. The splitting characterizing the band crossing the Fermi energy reaches a maximum of 48meV , as shown in Fig.3 (b), which is larger than 38meV , the maximum value reported for the half-fluorinated graphene C_2F [46]. For the bands located at the Fermi level, Fig.4 reveals that the Wannier functions, obtained from the projection of the p_z orbitals on the non-fluorinated Ge-atoms, are positioned at the centre of these atoms. The spread value of 2.04 indicates the delocalization of the Wannier function in real space. Besides, as shown in Fig.4, the Wannier functions overlap on three nearest neighboring (NN) germanium decorated sites, giving rise to the Coulomb contribution to the total

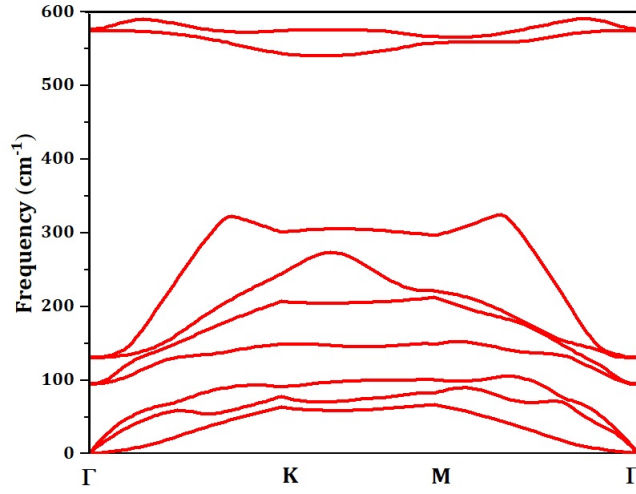


Figure 2: Phonon dispersion spectra calculated for the half fluorinated germanene.

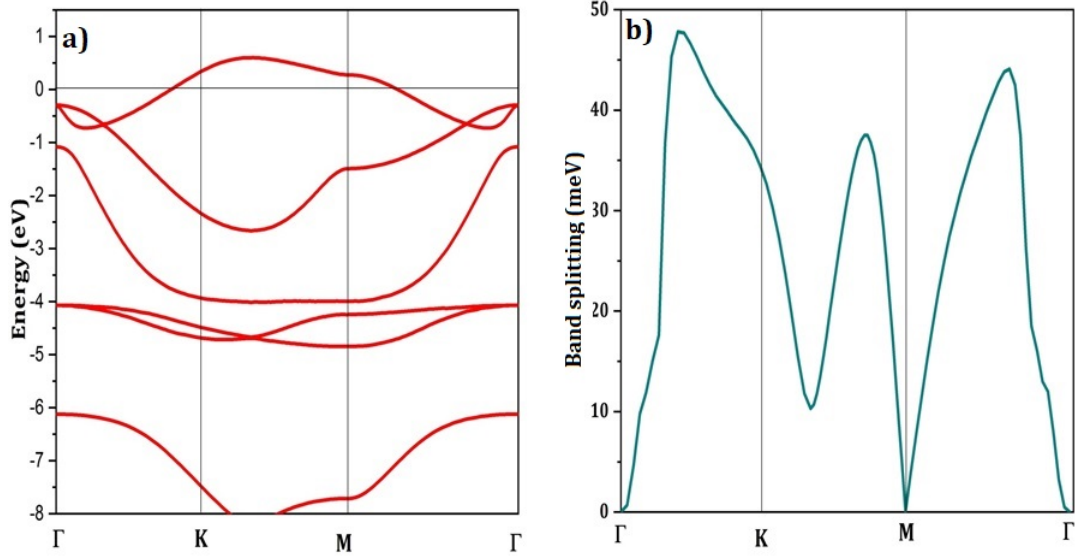


Figure 3: (a) The LDA band-structure with respect to the Fermi energy of half fluorinated germanene including spin-orbit coupling. Similarly to Ref. [46], the impact of spin-orbit coupling on the band crossing the Fermi energy is monitored in terms of the band splitting (b).

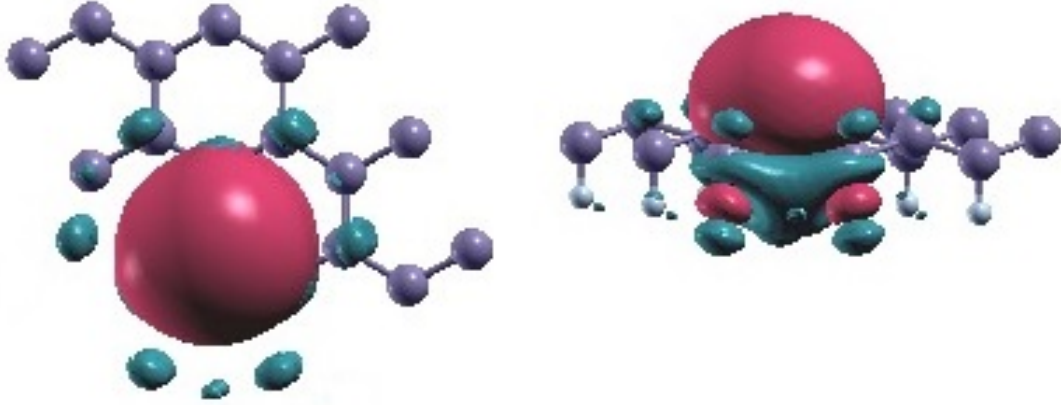


Figure 4: Representation of Maximally-Localized Wannier functions obtained from the projection of the p_z band at the Fermi level on the non-decorated Ge.

exchange interaction. The spin up/down channel of the partial density of states, displayed in Fig. 5, shows that the magnetism, which is relevant for Ge_2F near the Fermi level, is principally originated from p_z orbitals of the non-functionalized Ge atoms. This is due to the broken π – bonding network of pure non magnetic germanene. More precisely, in Ge_2F , the F-atoms form strong bonds with saturated Ge-atoms leaving p_z electrons of the non-decorated Ge-atoms free and localized. Within the ab-initio formalism, we explored various magnetic configurations of Ge_2F , namely, antiferromagnetic (AFM), ferromagnetic (FM), and ferrimagnetic (FI), utilizing the 4×4 supercell shown in the Fig. 6. The AFM state is found to be the lowest in energy. The energy differences with respect to the non-magnetic (NM) state are: $E_{\text{NM}} - E_{\text{AFM}} = 16.93$ meV, $E_{\text{NM}} - E_{\text{FI}} = 15.78$ meV and $E_{\text{NM}} - E_{\text{FM}} = 10.85$ meV. Owing to the presence of spin-orbit coupling, the hopping integrals are 2×2 matrices in spin-space. They are

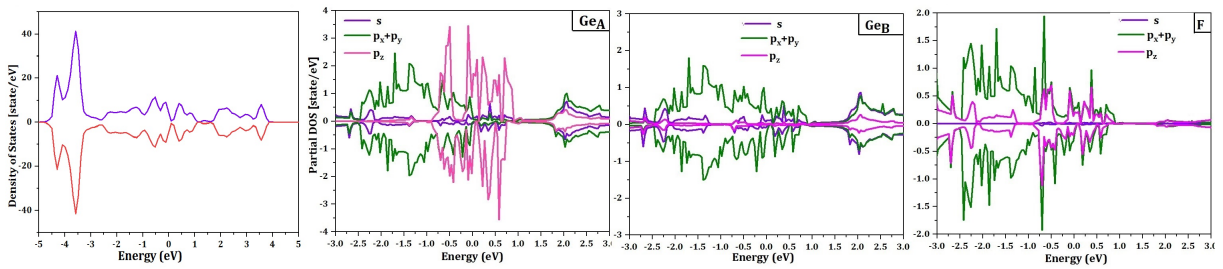


Figure 5: Totale density of states (DOS) and Partial density of states of half-fluorinated germanene as obtained with the antiferromagnetic (AFM) state described in the main text and shown in Fig. 6. The upper panel corresponds to the majority-spin (up) channel, while the lower one hosts the minority-spin (down) channel.

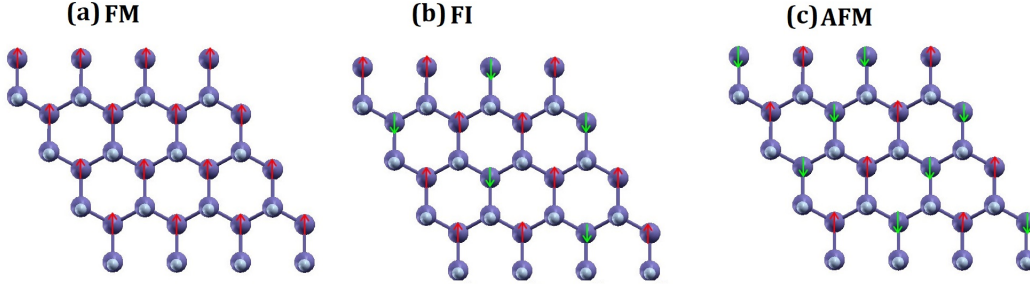


Figure 6: Three possible magnetic configurations of half-fluorinated germanene: (a) ferromagnetic , (b) ferrimagnetic and (c) antiferromagnetic, as explored from ab-initio.

listed below in meV for the case of first NN (01), second NN (02) and third NN (03) germanium atoms (see the schematic representation in Fig. 7(a)):

$$\begin{aligned}
 t_{01} &= \begin{bmatrix} -180.35 + 1.25i & 2.012 - 3.39i \\ -2.02 - 3.39i & -180.35 - 12.5i \end{bmatrix}, \\
 t_{02} &= \begin{bmatrix} 11.76 + 0.11 & 0.51 - 0.88i \\ -0.51 - 0.88i & -11.758 - 0.11i \end{bmatrix}, \\
 t_{03} &= \begin{bmatrix} 20.18 & -1.3 + 0.75i \\ 1.3 + 0.75i & 20.18 \end{bmatrix}.
 \end{aligned}$$

We note that (i) the hopping matrix between the first nearest neighbors contain large imaginary and non-diagonal elements, which are responsible for the antisymmetric anisotropic exchange interactions (DMI), and (ii) $t_{ij} \ll U$. In this case, Heisenberg Hamiltonian can be constructed within the superexchange theory [69] as follows [70]:

$$\hat{H} = \sum_{ij} J_{ij} \hat{m}_i \hat{m}_j + \sum_{ij} \mathbf{D}_{ij} [\hat{m}_i \times \hat{m}_j] \quad (5)$$

where $\hat{m} = \frac{\mathbf{M}}{|\mathbf{M}|}$ is the classical Heisenberg vector of unit length, J_{ij} and \mathbf{D}_{ij} are the isotropic exchange coupling and the DMI vector, respectively. The summation runs twice over all pairs.

3.1 Isotropic exchange interaction

A mapping of the previous Heisenberg Hamiltonian to eq. 1 leads to the following form of the isotropic exchange interaction:

$$J_{ij} = \frac{1}{\tilde{U}} \text{Tr}_\sigma \{ \hat{t}_{ji} \hat{t}_{ij} \} - J_{ij}^F \quad (6)$$

where \hat{t}_{ij} is the hopping energy taking into account spin-orbit coupling and $\tilde{U} = U_{00} - U_{01}$ [46] corresponds to the effective local partially-screened Coulomb interaction calculated via constrained random phase approximation (cRPA) [52]. U_{ij} and J_{ij}^F , with $i \neq j$, are often much smaller than U_{00} , which usually motivates their neglect. However, Mazurenko et al. [46] has shown that J_{ij}^F needs to be taken into account when extracting the magnetic exchange interactions in C_2F and C_2H . Our analysis of the case of Ge_2F shows that in contrast to C_2F , the non-local J_{ij}^F are negligible. This can

bond	radius vectors	$D_{ij}(meV)$
0 - 1'	$\left(\frac{1}{2}, -\frac{\sqrt{3}}{2}, 0.0\right)$	$\left(-0.65, -0.38, 0.242\right)$
0 - 1''	$\left(\frac{1}{2}, \frac{\sqrt{3}}{2}, 0.0\right)$	$\left(0.65, -0.38, 0.242\right)$
0 - 1	$\left(1, 0, 0\right)$	$\left(0.00, -0.753, -0.242\right)$

Table 1: The Dzyaloshinskii-Moriya vectors

be explained by the extremely weak spin-polarization of the non-fluorinated Ge atoms, which play an important role in mediating the interactions between the fluorinated Ge atoms [65]. The local Coulomb interaction U_{00} and non local Coulomb interaction U_{01} are respectively equal to $2.80eV$ and $0.92eV$, which leads to $\tilde{U} = 1.88eV$. The first term in equation 6 represents the Anderson superexchange, while the non-local J_{ij}^F is the ferromagnetic term that could originate from the direct overlap of the neighboring Wannier functions. In contrast to C_2F [46], however, J_{ij}^F is rather negligible in Ge_2F because of the weak magnetic moment carried by germanium. Therefore, we use in practice the usual form:

$$J_{ij} = \frac{1}{\tilde{U}} Tr_{\sigma} \left\{ \hat{t}_{ji} \hat{t}_{ij} \right\} \quad (7)$$

Using LDA+SO calculations by integrating the corresponding combination of the Wannier functions, one deduces that the isotropic exchange interaction between the first nearest neighbors $J_{01} = 1.4$ meV is very important when compared to the second nearest neighbors $J_{02} = 0.11$ meV and the third nearest neighbors $J_{03} = 0.15$ meV. The positive sign J_{01} confirms that the half fluorinated-germanene is antiferromagnetic.

3.2 Dzyaloshinskii-Moriya interaction

The anisotropic exchange interaction resulting from the spin-orbit interaction, is expressed as follows:

$$\mathbf{D}_{ij} = -\frac{i}{2\tilde{U}} \left[Tr_{\sigma} \left\{ \hat{t}_{ji} \right\} Tr_{\sigma} \left\{ \hat{t}_{ij} \sigma \right\} - Tr_{\sigma} \left\{ \hat{t}_{ij} \right\} Tr_{\sigma} \left\{ \hat{t}_{ji} \sigma \right\} \right] \quad (8)$$

where σ are the Pauli matrices. For the nearest neighbour bonds in Ge_2F , the DMI vectors as well as the radius vectors are presented in Table 1 and Fig. 7. In general, the orientation of DMI is defined by the symmetries of the crystal. In our case, the spin Hamiltonian symmetry is consistent with the C_{3v} point group of the triangular lattice formed by non-functionalized Ge atom as shown in Fig.7-b. The vertical reflections pass through the middle of bonds between the nearest neighbours. Furthermore, the corresponding DMI vectors lie in the reflection planes and are perpendicular to the interatomic bonds. The z-components of the DMI vector can change sign depending on the pair of nearest neighboring atoms.

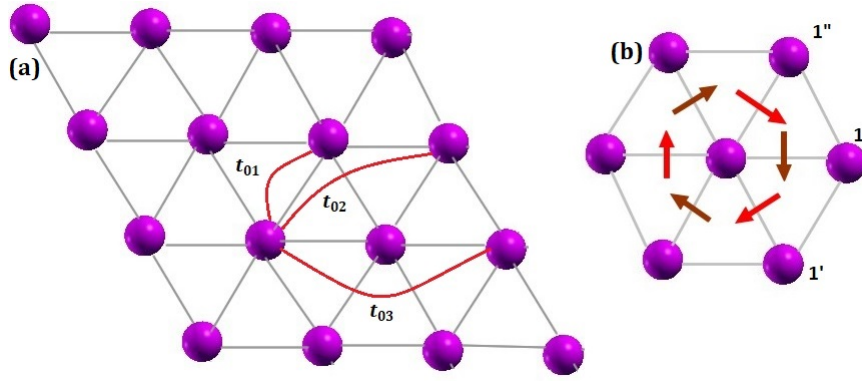


Figure 7: Schematic representation of (a) Hopping paths and (b) Dzyaloshinskii-Moriya vectors for half fluorinated germanene. Dark and light red arrows are DM-vectors with negative and positive z -components, respectively.

Figure 8: (a) The ground state of half fluorinated germanene (Ge_2F) is a Néel antiferromagnetic state. The spins lay in the film plane due to the z -components of the Dzyaloshinskii-Moriya vectors ($E = -23.21$ meV/atom). (b) Applying an external field (4000 T) along the x -direction (to the right-hand side), a Néel distorted state is obtained ($E = -38.63$ meV/atom). (c-d) Under the influence of the same external field, metastable spin-spiral states can be obtained ($E = -38.41$ and $E = -38.35$ meV/atom, respectively).

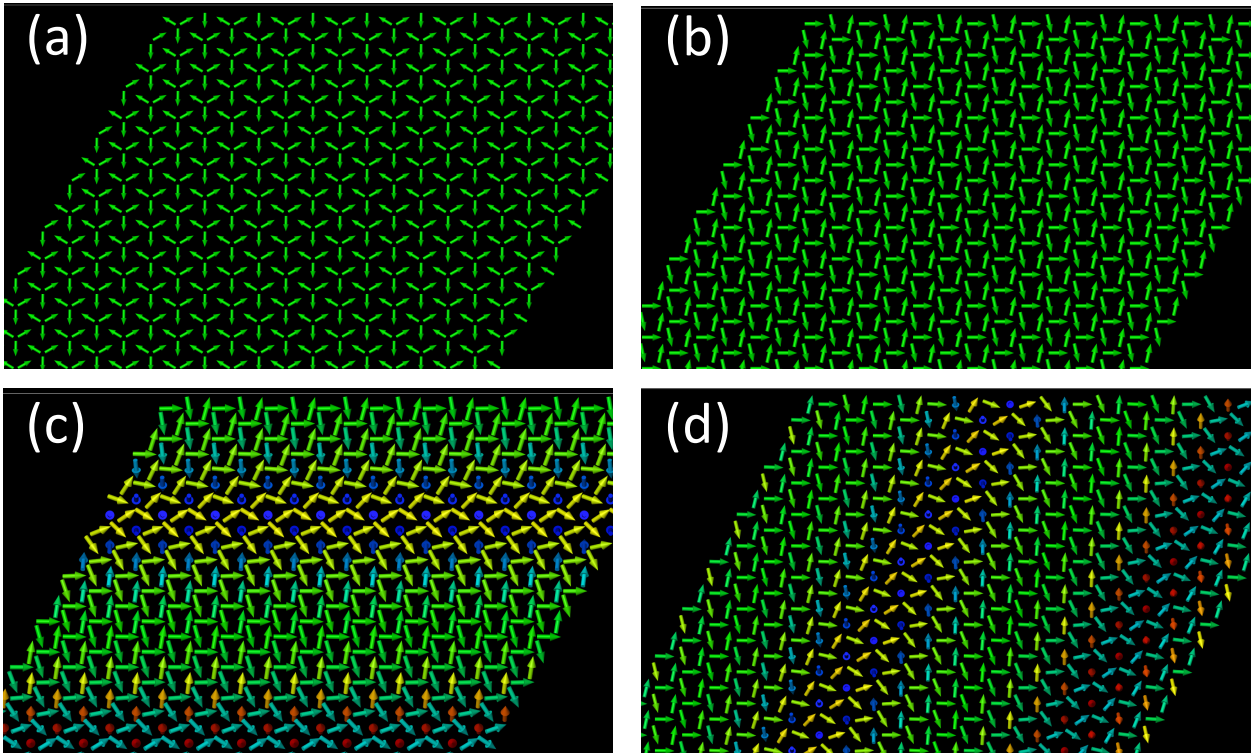
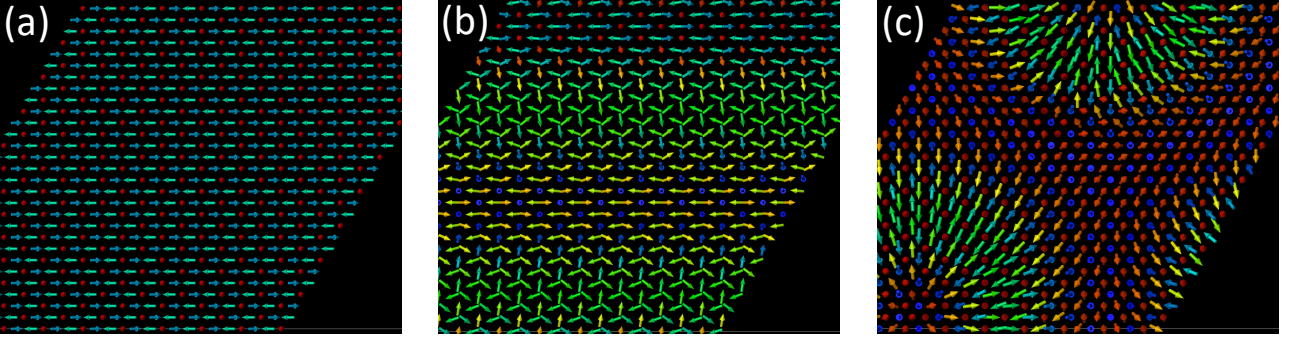


Figure 9: (a) Ground state of half fluorinated germanene (Ge_2F) when the out-of-plane components of the Dzyaloshinskii-Moriya vectors are disregarded (energy of -21.97 meV/atom). The spins lay in the $x - z$ plane. (b) Even in the absence of external, spin-spiral states can be obtained (energy of -21.942 meV/atom). (c) Applying an external field of 2000 T along the z -direction (to the right-hand side), an antiferromagnetic skyrmion lattice is formed (energy of -25.897 meV/atom).



3.3 Spin-dynamics simulations

After solving the LLG equation, Eq. 2, utilizing the extracted magnetic exchange interactions, we obtained as the ground state a Néel state with a zero net magnetization as shown in Fig. 8(a). The nearest neighboring AFM interactions favor the realization of such a magnetic state. Interestingly, we find that the z -component of the DMI imposes to have the moments in the surface plane. If one removes the z -component of the DMI, the resulting Néel state is characterized by out-of-plane components of the magnetic moments (Fig. 9(a)). In this particular case, a metastable spin-spiral state can be stabilized (Fig. 9(b)) which has an energy of 0.031 meV/atom above that of the ground state.

When applying a large magnetic field (up to 4000 T) along the x -axis, applied to the right in Fig. 8(b), a modified Néel state is obtained if keeping the z -component of the DMI finite. However, one can also obtain at higher energies the spin spirals shown in Figs. 8(c-d). Without the z -component of the DMI, an antiferromagnetic skyrmion can even be stabilized with a field of 2000 T along the z -axis (Fig. 8(c)). We conjecture that such large magnetic fields can be induced via a proximity effect if the 2D material is deposited on a magnetic substrate. The equivalent magnetic exchange energy for the 2000 T field is 32.41 meV, which could potentially be accessed. The spin-excitations spectra corresponding to the Néel ground state [Fig. 8(a)] as they would be measurable with SREELS or EELS are depicted in Figs. 10(a-d). We computed the spectra along the Brillouin-zone path indicated in Fig. 10(e). Figure 10(d) shows the total inelastic spectrum as they would be probed by an unpolarized electronic beam. Notice the strong scattering intensities around the K point and the vanishing intensities at the Γ , which are common spectroscopy features of antiferromagnets [58, 59]. We can count up to three spin-wave branches which can be individually detected through the spin-resolved spectroscopy. Figure 10(a-c) represent the spin-resolved spectra that arise from the possible spin orientations of the incoming and outgoing electrons. We chose the polarization of the probing electrons perpendicular to the magnetic film. Figure 10(a) corresponds to the non-spin-flip scattering channels, such that when we send electrons with spin down we measure only scattered electrons with the same spin. The spectrum displays a single spin-wave branch with an energy minimum (100 meV) at the K point. In Fig. 10(b) and (c), we have the spectra for the excitations which require spin flips of the probing electrons. In

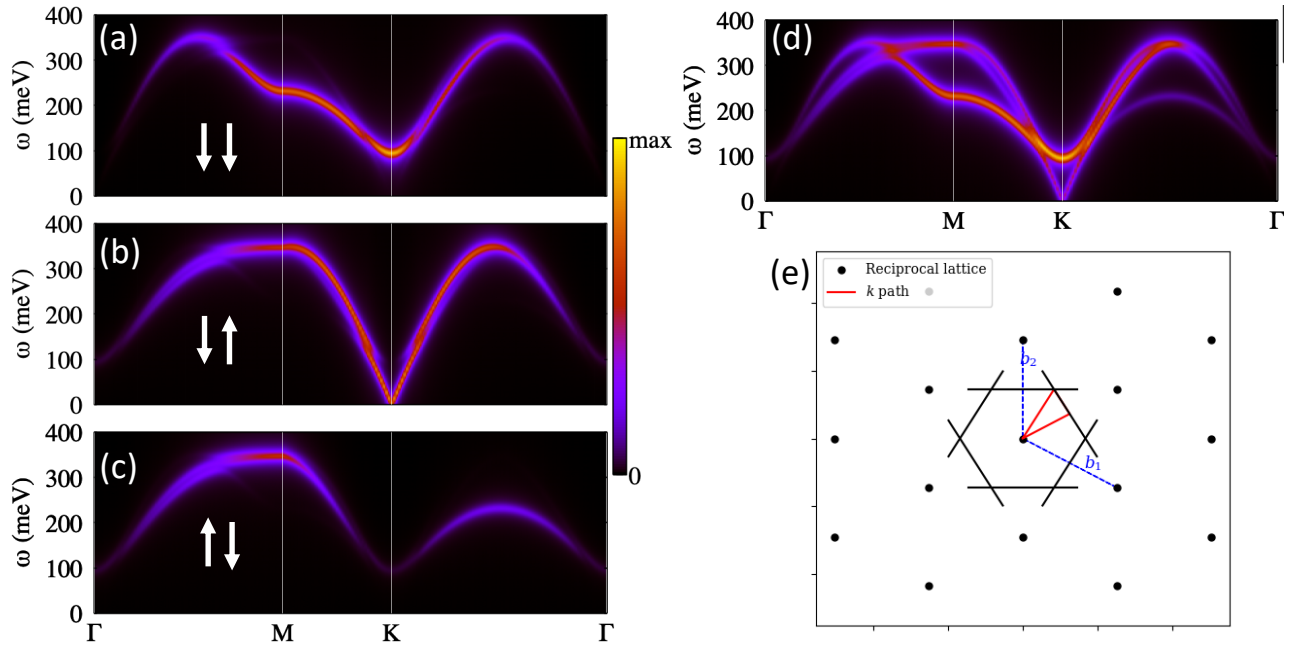


Figure 10: Inelastic electron scattering spectra for the Néel ground state. (a-c) show the spin-resolved scattering channels for probing electrons polarized perpendicularly to the surface. (a) corresponds to a non-spin-flip channel where we observe a linearly polarized mode (with zero net angular momentum). The spin-wave mode observed in (b) requires a spin-flip process. (d) displays the total spectrum that also corresponds to a spectroscopy with unpolarized electrons. The scattering spectra were calculated along the red path indicated in (e).

these processes, angular momenta is exchange between the probing electrons and the spin waves. The spin-wave mode in Fig. 10(b) has a linear dispersion at low energies, which are the characteristic spin-wave feature of antiferromagnets (see for example Ref. [59]).

4 Conclusion

To summarize our study, we performed an ab-initio investigation of the complex magnetic properties of a half-fluorinated Germanene (Ge_2F) and use a low-energy model to map the first-principles calculations and extract the magnetic exchange interactions as well as the Dzyaloshinskii-Moriya interaction vector. The latter is induced by the strong spin-orbit coupling of Germanium atoms and by the fact that the fluorine atoms break inversion symmetry.

The magnetic exchange interactions are antiferromagnetic among the first, second and third nearest neighbors, which stabilize a Néel state where the magnetic moments are lying in the surface plane. This particular configuration is favored by the out-of-plane component of the DMI vector. Antiferromagnetic spin spirals are found as metastable states once a magnetic field is applied. Interestingly, if the out-of-plane component of the DMI vector is set to zero, antiferromagnetic skyrmions can be found. For the realization of such chiral magnetic textures, we propose to use a potential magnetic substrate to induce the requested large magnetic fields. Finally, we explored for completeness the spin-waves excitations and presented the spectra that could be measurable with electron energy loss spectroscopy or its spin-resolved version.

acknowledgement

F. Z. Ramadan and L. B. Drissi would like to acknowledge "Académie Hassan II des Sciences et Techniques-Morocco" for financial support. L. B. Drissi acknowledges the Alexander von Humboldt Foundation for financial support via the George Forster Research Fellowship for experienced scientists (Ref 3.4 - MAR - 1202992). The work of F. J. dos Santos and S. Lounis was supported by the European Research Council (ERC) under the European Union's Horizon 2020 research and innovation programme (ERC-consolidator Grant No. 681405-DYNASORE). We gratefully acknowledge the computing time granted by JARA-HPC on the supercomputer JURECA at Forschungszentrum Jülich and by RWTH Aachen University.

References

- [1] V. Baltz, A. Manchon, M. Tsoi, T. Moriyama, T. Ono, and Y. Tserkovnyak. Antiferromagnetic spintronics. *Rev. Mod. Phys.*, **90** (2018) 015005.
- [2] T. Jungwirth, X. Marti, P. Wadley, and J. Wunderlich. Antiferromagnetic spintronics *Nature Nanotechnology* **11** (2016) 231-241.
- [3] P. Wadley, B. Howells, J. Železný, C. Andrews, and V. Hills, and R. P. Campion, et al. Electrical switching of an antiferromagnet, *Science* **351** (2016) 587-590.

- [4] K. Olejník, T. Seifert, Z. Kašpar, V. Novák, P. Wadley, R. P. Campion, et al. Terahertz electrical writing speed in an antiferromagnetic memory, *Science Advances* **4** (2018) eaar3566.
- [5] A. N. Bogdanov, and D. Yablonskii. Thermodynamically stable “vortices” in magnetically ordered crystals. The mixed state of magnets. *J. Exp. Theor. Phys.*, **95** (1989) 178.
- [6] U. K. Rössler, A. N. Bogdanov, and C. Pfleiderer. Spontaneous skyrmion ground states in magnetic metals. *Nature*, **442** (2006) 797-801.
- [7] S. Mühlbauer, B. Binz, F. Jonietz, C. Pfleiderer, A. Rosch, A. Neubauer, et al. Skyrmion lattice in a chiral magnet. *Science*. **323** (2017) 915-919.
- [8] W. Jiang¹, P. Upadhyaya, W. Zhang¹, G. Yu, M. B. Jungfleisch¹, F. Y. Fradin¹, et al. Blowing magnetic skyrmion bubbles. *Science* **8** (2015) 283-286.
- [9] Y. Zhou, and M. Ezawa. A reversible conversion between a skyrmion and a domain-wall pair in a junction geometry. *Nature Communications*. **1** (2014) 1-8.
- [10] H. Du, R. Che, L. Kong, X. Zhao, Ch. Jin, C. Wang, et al. Edge-mediated skyrmion chain and its collective dynamics in a confined geometry. *Nature Communications*. **6** (2015) 1-7.
- [11] J. Barker, and O.A. Tretiakov. Static and dynamical properties of antiferromagnetic skyrmions in the presence of applied current and temperature, *Physical Review Letters* **116** (2016) 147203.
- [12] H. Velkov, O. Gomonay, M. Beens, G. Schwiete, A. Brataas, J. Sinova, and R. A. Duine, Phenomenology of current-induced skyrmion motion in antiferromagnets, *Phys. Rev. B* **18** (2016) 075016.
- [13] R. Keesman, M. Raaijmakers, A. E. Baerends, G. T. Barkema, R. A. Duine, Skyrmions in square-lattice antiferromagnets, *Phys. Rev. B* **94** (2016) 054402
- [14] X. Zhang, Y. Zhou, and M. Ezawa, Antiferromagnetic skyrmion: stability, creation and manipulation, *Scientific reports* **6** (2016) 24795.
- [15] B. Göbel, A. Mook, J. Henk, and I. Mertig, Spin eigenexcitations of an antiferromagnetic skyrmion, *Physical Review B* **99** (2019) 184429.
- [16] V.P. Kravchuk, O. Gomonay, D. D. Sheka, D.R. Rodrigues, K. Everschor-Sitte, et al, Spin eigenexcitations of an antiferromagnetic skyrmion, *Physical Review B* **122** (2019) 184429.
- [17] Z. Liu, M. dos Santos Dias, and S. Lounis, Topological Magnons and Edge States in Antiferromagnetic Skyrmion Crystals, *Physical Review Letters* **122** (2019) 187203.
- [18] Z. Liu, M. dos Santos Dias, and S. Lounis, Theoretical investigation of antiferromagnetic skyrmions in a triangular monolayer, *Journal of Physics: Condensed Matter* **32** (2020) 425801.
- [19] N. Nagaosa and Y. Tokura. Topological properties and dynamics of magnetic skyrmions. *Nat. Nanotechnol.* **8** (2013) 899-911.

- [20] R. Wiesendanger. Nanoscale magnetic skyrmions in metallic films and multilayers: a new twist for spintronics. *Nature Reviews Materials*. **1** (2016) 16044.
- [21] A. Fert, N. Reyren, and V. Cros. Magnetic skyrmions: advances in physics and potential applications. *Nature Reviews Materials*. **2** (2016) 1-15.
- [22] X. Zhang, Y. Zhou, M. Ezawa, G.P. Zhao, and W. Zhao, Magnetic skyrmion transistor: skyrmion motion in a voltage-gated nanotrack, *Scientific reports*. **5** (2015) 11369.
- [23] Crum, M. Dax, M. Bouhassoune, J. Bouaziz, B. Schweflinghaus, S. Blügel, and S. Lounis, Perpendicular reading of single confined magnetic skyrmions, *Nature Commun*. **6** (2015) 1-8.
- [24] I. L. Fernandes, M. Bouhassoune, and S. Lounis, Defect-implantation for the all-electrical detection of non-collinear spin-textures, *Nature Commun*. **11** (2020) 1-9.
- [25] W. Kang, Y. Huang, C. Zheng, W. Lv, N. Lei, Y. Zhang, et al. Voltage controlled magnetic skyrmion motion for racetrack memory, *Scientific reports*. **6** (2016) 23164.
- [26] E. J. Kan, H. J. Xiang, F. Wu, C. Tian, C. Lee, J. L. Yang, et al. Monolayer honeycomb structures of group-IV elements and III-V binary compounds: First-principles calculations. *Physical Review B*. **15** (2010) 155453.
- [27] L. B. Drissi, N. B. Kanga, S. Lounis, F. Djeflal, and S. Haddad, Electron-phonon dynamics in 2D carbon based-hybrids XC (X= Si, Ge, Sn). *Journal of Physics: Condensed Matter*. **31** (2019) 135702.
- [28] W. Yao, D. Xiao, and Q. Niu, Valley-dependent optoelectronics from inversion symmetry breaking. *Physical Review B*. **77** (2019) 235406.
- [29] J. Liu, M. Shi, J. Lu, and M. P. Anantram, Analysis of electrical-field-dependent Dzyaloshinskii-Moriya interaction and magnetocrystalline anisotropy in a two-dimensional ferromagnetic monolayer. *Physical Review B*. **97** (2019) 054416.
- [30] K. K. Bai, Y. C. Wei, J. B. Qiao, S. Y. Li, L. J. Yin, W. Yan, et al. Detecting giant electron-hole asymmetry in a graphene monolayer generated by strain and charged-defect scattering via Landau level spectroscopy. *Physical Review B*. **92** (2015) 121405.
- [31] L. B. Drissi, K. Sadki, M.H. Kourra, and M. Bousmina, Strain-engineering of Janus SiC monolayer functionalized with H and F atoms. *Physical Chemistry Chemical Physics*. **123** (2018) 185106.
- [32] S.C. Zhu, C. T. Yip, S. J. Peng, K. M. Wu, K. L. Yao, C. L. Mak, et al. Half-metallic and magnetic semiconducting behaviors of metal-doped blue phosphorus nanoribbons from first-principles calculations. *Physical Chemistry Chemical Physics*, **20** (2018) 7635-7642.
- [33] Y. Mao, H. Xu, J. Yuan, and J. Zhong. Functionalization of the electronic and magnetic properties of silicene by halogen atoms unilateral adsorption: a first-principles study. *Journal of Physics: Condensed Matter* **30** (2018) 365001.

- [34] M. Sun, Q. Ren, Y. Zhao, J. P. Chou, J. Yu, and W. Tang, Electronic and magnetic properties of 4d series transition metal substituted graphene: a first-principles study. *Carbon* **120** (2017) 265-273.
- [35] L.B. Drissi, F.Z. Ramadan, and S. Lounis. Halogenation of SiC for band-gap engineering and excitonic Functionalization. *Journal of Physics: Condensed Matter*. **29** (2017) 455001.
- [36] E. J. Kan, H. J. Xiang, F. Wu, C. Tian, C. Lee, J. L. Yang, et al. Prediction for room-temperature half-metallic ferromagnetism in the half-fluorinated single layers of BN and ZnO. *Applied Physics Letters*. **97** (2010) 122503.
- [37] Y. Ma, Y. Dai, M. Guo, C. Niu, L. Yu, and B. Huang. Magnetic properties of the semifluorinated and semihydrogenated 2D sheets of group-IV and III-V binary compounds. *Applied Surface Science*. **257** (2018) 7845-7850.
- [38] H. M. Le, T. T. Pham, T. S. Dinh, Y. Kawazoe, and D. Nguyen-Manh. First-principles modeling of 3d-transition-metal-atom adsorption on silicene: a linear-response DFT+ U approach. *Journal of Physics: Condensed Matter*. **28** (2016) 135301.
- [39] F. Marsusi, N. D. Drummond, and M. J. Verstraete. The physics of single-side fluorination of graphene: DFT and DFT+ U studies . *Applied Surface Science*. **144** (2019) 615-627.
- [40] J. Zhou, Q. Wang, Q. Sun, and P. Jena. Electronic and magnetic properties of a BN sheet decorated with hydrogen and fluorine. *Physical Review B*. **8** (2010) 085442.
- [41] D. I. Badrtdinov, S. A. Nikolaev, A. N. Rudenko, M. I. Katsnelson, and V. V. Mazurenko. Nanoskyrmion engineering with s p-electron materials: Sn monolayer on a SiC (0001) surface. *Physical Review B*. **98** (2018) 184425.
- [42] F. B. Zheng, and C. W. Zhang. The electronic and magnetic properties of functionalized silicene: a first-principles study. *Nanoscale research letters*. **144** (2012) 1-5.
- [43] W. X. Zhang, Y. B. Wang, P. Zhao, and C. He. Tuning the electronic and magnetic properties of graphene-like SiGe hybrid nanosheets by surface functionalization. *Physical Chemistry Chemical Physics*. **18** (2016) 26205-26212.
- [44] L. B. Drissi, F. Z. Ramadan, and N. B-J Kanga. Fluorination-control of electronic and magnetic properties in GeC-hybrid. *Chemical Physics Letters*. **659** (2016) 148-153.
- [45] A. N. Rudenko, F. J. Keil, M. I. Katsnelson, and A. I. Lichtenstein. Exchange interactions and frustrated magnetism in single-side hydrogenated and fluorinated graphene. *Phys. Rev. B*, **88** (2013) 081405.
- [46] A. N. Mazurenko, S. A. Rudenko, D. S. Nikolaev, A. Medvedeva, I. Lichtenstein, and M. I. Katsnelson. Role of direct exchange and Dzyaloshinskii-Moriya interactions in magnetic properties of graphene derivatives: C_2F and C_2H . *Physical Review B*. **94** (2016) 214411.

- [47] Y. Ma, M. Dai, M. Guo, C. Niu, L. Yu, and B. Huang. Strain-induced magnetic transitions in half-fluorinated single layers of BN, GaN and graphene. *Nanoscale*. **3** (2011) 2301-2306.
- [48] L. B. Drissi, F.Z. Ramadan, E.H. Saidi, M. Bousmina, and O. F-Fehri. Fluorination effects on electronic and magnetic properties of silicene graphene hybrids . *Journal of the Physical Society of Japan*. **82** (2013) 104711.
- [49] J. Cenker, B. Huang, N. Suri, P. Thijssen, A. Miller, T. Song, et al. Direct observation of two-dimensional magnons in atomically thin CrI_3 , *Nature Physics* (2020) 1-6.
- [50] D. R. Klein, D. MacNeill, J. L. Lado, D. Soriano, E. N-Moratalla, K. Watanabe, et al. Probing magnetism in 2D van der Waals crystalline insulators via electron tunneling, *Nature Physics*, **360** (2018) 1218-1222.
- [51] P. Giannozzi, S. Baroni, N. Bonini, M. Calandra, R. Car, C. Cavazzoni, et al. QUANTUM ESPRESSO: a modular and open-source software project for quantum simulations of materials. *Journal of physics: Condensed matter*. **21** (2009) 395502.
- [52] B. Amadon, T. Applencourt, and F. Bruneval. Screened Coulomb interaction calculations: cRPA implementation and applications to dynamical screening and self-consistency in uranium dioxide and cerium. *Physical Review B*. **89** (2014) 125110.
- [53] X. Gonze, F. Jollet, F. A. Araujo, D. Adams, B. Amadon, T. Applencourt, et al. Recent developments in the ABINIT software package. *Computer physics communications*. **205** (2016) 106-131.
- [54] A. A. Mostofi, J. R. Yates, Y. S. Lee, I. Souza, D. Vanderbilt, and N. Marzari . Wannier90: A tool for obtaining maximally-localised Wannier functions. *Computer physics communications*. **178** (2008) 685-699.
- [55] G. P. Müller, M. Hoffmann, C. Dißelkamp, D. Schürhoff, S. Mavros, M. Sallermann, N. S. Kiselev, H. Jónsson, and S. Blügel. Spirit: Multifunctional framework for atomistic spin simulations. *Physical Review B*. **99** (2019) 224414.
- [56] F. J. Dos Santos, M. dos Santos Dias, and S. Lounis, First-principles investigation of spin-wave dispersions in surface-reconstructed Co thin films on W(110), *Physical Review B* **95** (2017) 134408.
- [57] F. J. Dos Santos, M. dos Santos Dias, F. S. M. Guimarães, J. Bouaziz, and S. Lounis, Spin-resolved inelastic electron scattering by spin waves in noncollinear magnets, *Physical Review B* **97** (2018) 024431.
- [58] F. J. D. Santos, M. D. S. Dias, and S. Lounis, Nonreciprocity of spin waves in noncollinear magnets due to the Dzyaloshinskii-Moriya interaction, *Scientific reports*. (2020) **arXiv:2003.11649**.
- [59] F. J. D. Santos, M. D. S. Dias, and S. Lounis, Voltage controlled magnetic skyrmion motion for racetrack memory, *Scientific reports*. (2020) **arXiv:2005.07250**.

- [60] P. Liang, Y. Liu, S. Xing, H. Shu, and B. Tai. Electronic and magnetic properties of germanene: surface functionalization and strain effects. *Solid State Communications*, **226** (2016) 19-24.
- [61] S. Sun, F. Meng, H. Wang, H. Wang, Y. Ni. Novel two-dimensional semiconductor SnP 3: high stability, tunable bandgaps and high carrier mobility explored using first-principles calculations. *Journal of Materials Chemistry A*, **6** (2018), 11890-11897.
- [62] M. Ashton, J. Paul, S.B. Sinnott, and R.G. Hennig. Topology-scaling identification of layered solids and stable exfoliated 2D materials. *Physical review letters*, **118** (2017) 106101
- [63] P. Avramov, V. Demin, M. Luo, C.H. Choi, P.R. Sorokin, B. Yakobson, and L. Chernozatonskii. Translation symmetry breakdown in low-dimensional lattices of pentagonal rings. *The journal of physical chemistry letters*, **6**(2015), 4525-4531.
- [64] A. V. Kuklin, H. Agren, P.V. Avramov. Structural stability of single-layer *PdSe₂* with pentagonal puckered morphology and its nanotubes. *Physical Chemistry Chemical Physics*, **22**(2020), 8289-8295.
- [65] V. V. Mazurenko, S. L. Skornyakov, V. I. Anisimov, and F. Mila, , First-principles investigation of symmetric and antisymmetric exchange interactions of $\text{SrCu}_2(\text{BO}_3)_2$, *Phys. Rev. B* **7** (2008) 195110.
- [66] M. Goli, S.M. Mozvashi, P. Aghdasi, S. Yousefi, and R. Ansari. A DFT study on the mechanical properties of hydrogenated and fluorinated germanene sheets. (2020) arXiv preprint arXiv:2005.07583.
- [67] L. B. Drissi, and F. Z. Ramadan. Many body effects study of electronic and optical properties of silicene-graphene hybrid. *Physica E: Low-dimensional Systems and Nanostructures* **68** (2015) 38-41.
- [68] L. B. Drissi, F. Z. Ramadan, Excitonic effects in GeC hybrid: Many-body Green's function calculations. *Physica E: Low-dimensional Systems and Nanostructures*, **74** (2015)377-381.
- [69] P. W. Anderson. Anisotropic spin Hamiltonians due to spin-orbit and Coulomb exchange interactions. *Physical Review*, **115** (1959) 2-13.
- [70] T. Yildirim, A. B. Harris, A. Aharony, and O. Entin-Wohlman. Anisotropic spin Hamiltonians due to spin-orbit and Coulomb exchange interactions. *Phys. Rev. B*, **52** (1995) 10239-10267.